Proceedings of IMECE04
2004 ASME International Mechanical Engineering Congress and Exposition
November 13-20, 2004, Anaheim, California USA

IMECE2004-60927

A 1-D PLANAR SOLID OXIDE FUEL CELL MODEL FOR SIMULATION OF SOFC-BASED ENERGY SYSTEMS

Marco Sorrentino[1]*, Ashraf Mandourah, Thomas F. Petersen**, Yann G. Guezennec, Michael J. Moran (ASME Fellow) and Giorgio Rizzoni

Department of Mechanical Engineering, The Ohio State University, Columbus, Ohio 43210
* Department of Mechanical Engineering, University of Salerno, Fisciano, Italy
** Department of Mechanical Engineering, Technical University of Denmark, Lyngby, Denmark

ABSTRACT

A one-dimensional steady-state model for planar solid oxide fuel cells (SOFCs) is presented. Appropriately simplified, the model includes sufficient detail for supporting ongoing investigations involving the simulation of SOFC-based advanced energy systems. The presentation focuses on a set of nonlinear equations accounting for conservation of mass and energy along a single SOFC in a co-flow configuration. Electrochemical models also are employed, including one previously used for a zero dimensional approach. The equations are described through a phenomenological approach based on the best recent work in the field and model validation is carried out in two distinct phases using previously published information. Potential areas of application for the model presented are noted.

INTRODUCTION

The objective of this paper is to report on work in progress aimed at simulating advanced energy systems having a solid oxide fuel cell as a principal component. For such work it is sufficient to employ a simplified SOFC model that captures the salient physical/chemical effects. Accordingly, efforts thus far have centered on the development of a one-dimensional SOFC model resting solidly on the best recent work in the field, while being convenient and effective for achieving the larger goal of simulating SOFC-based advanced energy systems. The intent of this modeling effort is to be able to handle both the hydrogen and internal reforming cases, while representing the electrochemistry using either a grey box approach or black box approach.

Specifically in this paper, a 1-D model has been developed that captures the dominant physical and electrochemical phenomena taking place in a co-flow planar SOFC, accounting for internal reforming while retaining computational simplicity and good accuracy. The objective of the model is to simulate and predict the performance of a single fuel cell under a variety of operating conditions. The resulting performance data would serve as the basis for defining a fuel cell component that would be integrated in a system-level simulation model that includes the balance of the plant and system integration particularly towards automotive or military applications.

The model accuracy is verified by comparing the model outputs with those published in previous works [1, 2]. Due to the lack of reference data that comprehensively cover the typical operational domain of a SOFC, the model accuracy is verified through separate validation of the electrochemical and the energy balance sub-models. The experimental tests conducted by the Pacific Northwest National Laboratory (PNNL) [2] have been used to check the electrochemical model, whereas the energy aspect is analyzed referring to the special case of a "virtual" unit, whose specifications have been defined by the International Energy Agency (IEA) [1].

NOMENCLATURE

Symbol	Name and unit
A_{slice}	Electroactive area of an individual slice [cm^2]
A_s	Heat exchange surface area [cm^2]
E_{nernst}	Ideal potential [V]
E_{act}	Activation energy [J/mole]
$\dot{E}$	Energy rate [W]
$\dot{E}_{el}$	Electric power [W]
G	Standard Gibbs free energy [J/mol]
F	Faraday's constant [96485.34 C /mol]
h	Molar specific enthalpy [J/mol]
$\overline{h}$	Convective heat transfer coefficient [W/cm^2/K]
I	Current [A]
J	Current Density [A/cm^2]
k_i	Thermal conductivity of pure species i [W/cm/K]

[1] Corresponding author,
E-mail address: msorrentino@unisa.it (M. Sorrentino).

l_{ch}	Channel length [m]
l_c, l_a	Electrode thickness [cm]
l_e	Electrolyte thickness [cm]
M	Molar weight [g/mol]
N	Number of discrete slices [/]
n_e	Number of transferred electrons [/]
$\dot{n}_y$	Molar flow rate of the *yth* specie [mol/s]
P	Total pressure [bar]
p_y	Partial pressure of the *yth* specie [bar]
$\dot{q}$	Heat flux [W/cm^2]
$\dot{r}$	Reaction rate [mol/s]
R_u	Ideal gas constant [8.3144 J/mol/K]
T	Temperature [K]
U_f	Fuel utilization [/]
V	Voltage [V]
$\overline{V}$	Atomic diffusion volume [Å^3]
V_v	Electrode porosity [%]
w_{ch}	Channel width [m]
x	Molar fraction [/]

Greek letters

B	Ratio between l_{ch} and w_{ch} [/]
Δ	Change
σ	Conductivity [Ω·cm]$^{-1}$
τ	Electrode tortuosity [/]

Subscripts

a	Air
an	Anode
ca	Cathode
ch	Channel
ref	Methane reforming reaction
cons	Consumed
conv	Convective
f	Fuel
in, out	Inlet, outlet
ox	Oxidation reaction
prod	Reaction products
reac	Reactants
s	Solid trilayer
sto	Stoichiometric
shift	Water gas shift reaction

Super-scripts

i	*i-th* computational slice

SOLID OXIDE FUEL CELLS

For a methane-fed SOFC, the reactions include reforming of methane, oxidation of hydrogen, oxygen reduction and water-gas shift reaction. These simultaneous reactions, with the accompanying heat generation in the solid trilayer (anode-electrolyte-cathode), make the modeling of such SOFCs a challenging task. Numerous works in the literature have addressed mathematical modeling of planar SOFCs, e.g., [1, 3-6].

As shown in Figure 1, a SOFC consists of three components - a cathode, an anode, and an ion-conducting electrolyte separating the two electrodes. Air flows through the cathode, and a hydrogen-rich fuel gas flows past the anode. If methane is used, thanks to the very high operating temperatures (700 - 1000 °C), the fuel is internally reformed at the anode in the presence of steam to form carbon dioxide and hydrogen.

At the cathode, oxygen reduction takes place (eq. 1). The generated oxygen ions migrate through the electrolyte and react with the hydrogen at the anode to form water (eq. 2). This electrochemical reaction releases electrons, which flow back to the cathode through the external circuit providing electric power, as shown in Figure 1.

$$\frac{1}{2}O_2 + 2e^- \rightarrow O^{--} \qquad (cathode) \tag{1}$$

$$H_2 + O^{--} \rightarrow H_2O + 2e^- \quad (anode) \tag{2}$$

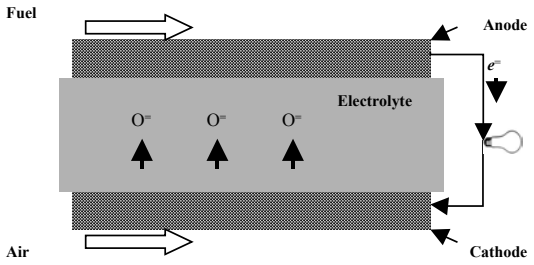

Figure 1 – Schematic of SOFC basic operation.

An important issue for fuel cells is the amount of fuel to be fed for proper operation. The ratio between the hydrogen required meeting the power demand and the amount to be fed defines the system Fuel Utilization (U_f). For a pure H_2-fueled case, U_f is defined as:

$$U_f = \frac{\dot{n}_{H_2,cons}}{\dot{n}_{H_2,in}} \tag{3}$$

In the case of methane, since for each mole of methane 4 moles of hydrogen can be produced via methane reforming and water-gas shift reactions, the fuel utilization can be expressed as:

$$U_f = \frac{\dot{n}_{H_2,cons}}{4 \cdot \dot{n}_{CH_4,in}} \tag{4}$$

Normally, SOFCs are air-cooled. The cooling flow of air coincides with the air flowing through the cathode. In order to preserve the cell component integrity, a large excess of air is required to limit the temperature increase within 100-150 °C. The Excess Air (EA) is defined as the ratio between the input air flow and the stoichiometric amount required to oxidize the hydrogen:

$$EA = \frac{\dot{n}_{O_2,in}}{\dot{n}_{O_2,sto}} = \frac{\dot{n}_{O_2,in}}{\frac{1}{2}\dot{n}_{H_2,cons}} = \frac{\dot{n}_{air,in}}{4.76 \cdot \frac{1}{2}\dot{n}_{H_2,cons}} \tag{5}$$

Previous studies indicate that to safely operate a SOFC system an excess air of about 7 suffices [1].

MODELING APPROACH

The 1-D modeling approach followed in this paper describes the main phenomena occurring inside a single co-flow planar SOFC. A detailed spatial description is needed since significant variations of temperature, current and partial pressures occur in the flow direction. At high temperatures, this spatial variability strongly affects the performance and the

efficiency achievable by the fuel cell. The use of a 1-D approach allows a more detailed physical description than a zero-dimensional one, thus enhancing and easing the identification and calibration of the polarization losses model. The higher physical detail level of the 1-D approach enables the definition of an accurate and flexible model accounting for the polarization losses as a function of different fuel types, cell dimensions and materials.

Modeling such phenomena entails solving the coupled energy, mass, and polarization equations as reported below. The developed model consists of a set of sub-models that are executed simultaneously in an iterative procedure in the Matlab environment utilizing its built-in optimization tool. The structure of the sub-models provides flexibility for executing and evaluating the contribution of each sub-model systematically. The 1-D model consists of a polarization sub-model, a material balance sub-model and an energy balance sub-model.

The model accounts for variations in the cell by dividing the domain into computational slices along the cell length, with the computation starting in the first slice at the inlet of the fuel/air flows and marching to the successive slices in the streamwise direction [1, 3]. At each computational slice, balances for mass, energy and electric potential are applied in order to derive a closed form. The cell is assumed to be isopotential [1]. Fully-stirred conditions are assumed at the slice level. Assuming uniform distribution but no mixing of air and fuel feed gases, the two streams are treated separately as perfect gases. Pressure drop across the fuel and air channels can be safely neglected [4]. Additional assumptions for each of the sub-models are considered below.

ELECTROCHEMICAL MODELS

As mentioned in the introduction, two different validation tests were carried out to assess the accuracy of the proposed model. For each case, a specific sub-model accounting for the polarization losses has been used. In this section, after a preliminary paragraph dedicated to the general form of the electrochemical model, the two polarization losses sub-models are presented.

General Form

The electrochemical sub-model evaluates the current, voltage and power of the SOFC. The model is phenomelogical and based on recent research on second-generation, anode-supported SOFCs [7].

For each slice i the current density is calculated by Faraday's law:

$$J^i = \frac{\dot{r}_{ox}^i \cdot F \cdot n_e}{A_{slice}^i} \tag{6}$$

By multiplying the current density of each slice by the slice area, the total current is found as a sum:

$$I_{SOFC} = \sum_{i=1}^{N} \left(J^i \cdot A_{slice}^i \right) \tag{7}$$

The ideal potential difference between the anode and cathode gases is evaluated using the Nernst equation:

$$E_{Nernst}^i = -\frac{\Delta G_{ox}^i(T_s^i)}{n_e F} - \frac{R_u T_s^i}{n_e F} \ln\left(\frac{p_{H_2O}^i}{p_{H_2}^i \sqrt{p_{O_2}^i}} \right) \tag{8}$$

There are three major forms of polarization losses: activation, ohmic and concentration. A minor constant offset polarization also contributes to the total polarization, which is the result of minor losses such as contact resistance, internal current and leaks. Following Chick et al. [8], a constant offset polarization of 0.07 volt has been assumed.

The sum of the different polarizations causes a voltage drop from the ideal Nernst potential to the operating voltage. Since the interconnect and the electrodes are assumed to be isopotential, the voltage is constant over the whole cell and can be estimated as:

$$V_{SOFC} = E_{Nernst}^i - \Delta V_{Act}^i - \Delta V_{Ohm}^i - \Delta V_{Conc}^i - \Delta V_{Offset} \tag{9}$$

The total power drawn from the SOFC is calculated as:

$$\dot{E}_{el} = V_{SOFC} \cdot I_{SOFC} \tag{10}$$

where I_{SOFC} is given by eq. (7).

Activation polarization - PNNL

Activation polarization is non-linear and is evaluated from an approximation of the Butler-Volmer equation [9]:

$$\Delta V_{Act}^i = \frac{R \cdot T_s^i}{\alpha(T_s^i) \cdot F} \cdot \sinh^{-1}\left(\frac{J^i}{2 J_0(T_s^i)} \right) \tag{11}$$

where α is the charge transfer coefficient and J_0 is the exchange current density. The above parameters have been found fitting the experimental data provided in Chick *et al.* [2]. Then, the following temperature-dependent relationships [8] have been used to correlate α and J_0 with the temperature:

$$\alpha(T) = C_1 T_s^i + C_2 \tag{12}$$

$$J_0(T) = (C_3 T_s^i + C_4) \cdot e^{\left(\frac{-E_{act,J_0}}{R T_s^i} \right)} \tag{13}$$

The parameters C_1, C_2, C_3 and C_4 used in (12) and (13) have been identified by fitting the experimental voltage values corresponding to an average current density of 0.5 A/cm^2 and are shown in Table 1.

Table 1: Parameters for charge transfer coefficient and exchange current density.

Parameter	Value
C_1	$2.13 \cdot 10^{-3}$
C_2	-1.69
C_3	$-1.12 \cdot 10^{-3}$
C_4	9.48
$E_{act,J0}$	$7.905 \cdot 10^{-4}$

Ohmic polarization - PNNL

Ohmic polarization depends on the electronic conductivity of the anode and cathode, and the ionic conductivity of the electrolyte. For each part of the SOFC, the ohmic polarization is expressed as:

$$\Delta V^i_{ohm,k} = \frac{l_k}{\sigma_k(T^i_s)} \cdot J^i$$
$$\Delta V^i_{ohm} = \sum_k \Delta V^i_{ohm,k} \qquad k = [an, ca, el] \tag{14}$$

Since the conductivity of the metallic interconnect is many times greater than for other parts, its contribution to the ohmic polarization is neglected [7]. The conductivity is dependent on the temperature and the materials used in the SOFC. The conductivity of the anode, cathode and electrolyte can be found using expressions previously developed [2] for second-generation SOFC materials, as follows.

The conductivity of a Nickel-cermets anode is assumed to be constant with temperature but is corrected to account for the porosity of the anode.

$$\sigma_{an,eff} = \sigma_{an} \cdot \left(1 - 1.8 \cdot V_{v,an}\right) \tag{15}$$

The values of anode conductivity, tortuosity and porosity are listed in Table 2 as given by Chick *et al.* [8].

Table 2: Anode Conductivity and electrodes porosity and tortuosity [8].

Parameter	Value
σ_{an}	1000
$V_{v,an}$	0.3
$V_{v,ca}$	0.3
τ_{an}	2.5
τ_{ca}	2.5

The conductivity of a Strontium-doped Lanthanum Manganite (SLM) cathode is evaluated in this study as a function of the temperature:

$$\sigma_{ca}(T_s) = C_5 \cdot \left(T^i_s\right)^2 - \mathrm{C}_6 \cdot T^i_s + \mathrm{C}_7 \tag{16}$$

As in eq. (15) for the anode, the conductivity of the cathode is corrected to account for porosity:

$$\sigma_{ca,eff} = \sigma_{ca} \cdot \left(1 - 1.8 \cdot V_{v,ca}\right) \tag{17}$$

The conductivity of the Yttria-Stabilized Zirconia (YSZ) electrolyte is expressed as a second order polynomial, with coefficients obtained by fitting the reference data, as for the coefficients listed in Table 1:

$$\sigma_{el}(T_s) = C_8 \cdot (T^i_s - 273)^2 + C_9 \cdot (T^i_s - 273) + C_{10} \tag{18}$$

Table 3 lists the constants used in equations (16-18):

Table 3: Electrolyte-Conductivity formula parameters.

Parameter	Value
C_5	$1.169\ 10^{-4}$
C_6	-0.1943
C_7	222.6
C_8	$6.68\ 10^{-7}$
C_9	$7.462\ 10^{-4}$
C_{10}	0.2135

Concentration polarization - PNNL

As the fuel is depleted, there is a decrease of the Hydrogen partial pressure at the anode and the oxygen partial pressure at the cathode. The rate of the depletion depends on the magnitude of the current density. As the current density increases, the partial pressures decrease and eventually an insufficient amount of reactants will be transported to the electrodes. This increases the concentration polarization until the voltage is reduced to zero [7, 10]. The current densities at which this occurs are called the anode and cathode limiting currents.

As a consequence, concentration polarization, which occurs at all current densities, is dominant at high current density. Like activation polarization, concentration polarization is non-linear and is evaluated from the following expression [7]:

$$V^i_{Conc} = -\frac{RT^i_s}{2F} \cdot \left[\frac{1}{2}\ln\left(1 - \frac{J^i}{J_{cs}(T^i_s)}\right) + \ln\left(1 - \frac{J^i}{J_{as}(T^i_s)}\right) - \ln\left(1 - \frac{p^i_{H_2} \cdot J^i}{p^i_{H_2O} \cdot J_{as}(T^i_s)}\right)\right] \tag{19}$$

The anode and cathode limiting currents are evaluated as [1]:

$$J_{cs}(T) = \frac{2n_e F}{RT} \cdot \frac{p_{O_2} \cdot D_{eff,ca}}{l_{ca}} \tag{20}$$

$$J_{as}(T) = \frac{n_e F}{RT} \cdot \frac{p_{H_2} \cdot D_{eff,an}}{l_{an}} \tag{21}$$

The effective diffusion coefficients D_{eff} are found by correcting the binary diffusion constants to account for the tortuosity and porosity of the electrodes [8]:

$$D_{eff,ca}\left(T^i_s\right) = \frac{V_{v,ca} \cdot D_{O_2-N_2}}{\tau_{ca}} \tag{22}$$

$$D_{eff,an}\left(T^i_s\right) = \frac{V_{v,an} \cdot D_{H_2-H_2O}}{\tau_{an}} \tag{23}$$

The binary diffusion constants of eqs. (22), (23) are found from an empirical correlation reported by [11]:

$$\mathrm{D_{AB}}\left(T^i_s\right) = \frac{10^{-3} \cdot \left(T^i_s\right)^{1.75} \sqrt{1/M_A + 1/M_B}}{P \cdot \left(\overline{V}_A^{1/3} + \overline{V}_B^{1/3}\right)^2} \tag{24}$$

The diffusion volumes of the relevant species, $\overline{V}$, are given in Table 4.

Table 4 : Atomic diffusion volumes [11].

Species	Diffusion volume [Å^3]
H_2	7.07
H_2O	12.7
N_2	17.9
O_2	16.6

The concentration polarization model above is strictly valid for a pure hydrogen fueled SOFC as it only accounts for binary diffusion of two species. Nevertheless, the model structure can be reasonably extended to a reformate-fueled case, as addressed by previous work [1].

Black box polarization losses sub-model – IEA

For the IEA benchmark, a much simpler black box correlation is used for the evaluation of the polarization losses.

The activation and concentration losses are approximated as being equal to the ohmic loss of the electrolyte yielding:

$$V_{SOFC} = E^i_{Nernst} - \Delta V^i_{Ohm} - 2 \cdot \Delta V^i_{Ohm,el} \quad (25)$$

The conductivities of the anode, cathode and electrolyte have been estimated using the relationships suggested by the IEA, reported in Table 5.

Table 5 : Solid components conductivities – IEA [1].

Component conductivity $[\Omega \cdot m]^{-1}$	
Anode	$\frac{95 \cdot 10^6}{T^i_s} \cdot \exp\left(\frac{-1150}{T^i_s}\right)$
Cathode	$\frac{42 \cdot 10^6}{T^i_s} \cdot \exp\left(\frac{-1200}{T^i_s}\right)$
Electrolyte	$\frac{3.34 \cdot 10^4}{T^i_s} \cdot \exp\left(\frac{-10300}{T^i_s}\right)$
Bipolar plate	$\frac{9.3 \cdot 10^6}{T^i_s} \cdot \exp\left(\frac{-1100}{T^i_s}\right)$

As pointed out earlier, the IEA unit simulation and its simplistic black box polarization model summarized above was only used to verify the accuracy of the energy balance sub-model. This was required as the published comparison data and models using the PNNL electrochemical model were only for the isothermal case. In future work, the overall approach will be validated with experimental data provided by an industrial partner, but clearance for publishing these data has not been granted at the time of writing this paper.

CONSERVATION EQUATIONS

The model accounts for internal reforming of a reformate-fuel supplied at the anode side by a pre-reformer. The reformate-fuel, which typically consists of a mixture of H_2, CH_4, CO and H_2O, undergoes steam reforming of CH_4, conversion of CO to CO_2, and electrochemical oxidation of H_2. These reactions are expressed, respectively, as:

$$CH_4 + H_2O \rightarrow CO + 3H_2 \quad (26)$$

$$CO + H_2O \leftrightarrow CO_2 + H_2 \quad (27)$$

$$H_2 + \frac{1}{2}O_2 \rightarrow H_2O \quad (28)$$

The water gas shift reaction (eq. 27) is assumed to be in equilibrium, for which the equilibrium constant is expressed as:

$$K_{shift}(T^i_s) = \exp\left(\frac{-\Delta G_{shift}(T^i_s)}{R_u T^i_s}\right) \quad (29)$$

The equilibrium constant also can be expressed as a function of the species molar fractions, as follows:

$$K_{shift} = \frac{x_{H_2} \cdot x_{CO_2}}{x_{CO} \cdot x_{H_2O}} \quad (30)$$

Material Balance

By applying conservation of mass, the molar balance for the species in the fuel channel yields:

$$\begin{cases} \dot{n}^i_{H_2} = \dot{n}^{i-1}_{H_2} + 3 \cdot \dot{r}^i_{ref} + \dot{r}^i_{shift} - \dot{r}^i_{ox} \\ \dot{n}^i_{CH_4} = \dot{n}^{i-1}_{CH_4} - \dot{r}^i_{ref} \\ \dot{n}^i_{H_2O} = \dot{n}^{i-1}_{H_2O} - \dot{r}^i_{ref} - \dot{r}^i_{shift} + \dot{r}^i_{ox} \\ \dot{n}^i_{CO} = \dot{n}^{i-1}_{CO} + \dot{r}^i_{ref} - \dot{r}^i_{shift} \\ \dot{n}^i_{CO_2} = \dot{n}^{i-1}_{CO_2} + \dot{r}^i_{shift} \end{cases} \quad (31)$$

where $\dot{r}^i_{ref}$ and r^i_{CO} are, respectively, the reaction rates of the methane reforming (eq. 26) and water-gas shift (eq. 27) reactions. $\dot{r}^i_{ref}$ is expressed as:

$$\dot{r}^i_{ref} = K_0 \, p_{CH_4,o} \, f_e \, A_{slice} \, e^{-(E_{act,ref}/R_u T^i_f)} \quad (32)$$

The values for the factor K_0 and the activation energy, $E_{act,ref}$, are found in Achenbach and Riensche [12] and the equilibrium factor, f_e, is approximated as 1 [1]. r^i_{CO} is found by substituting the current slice molar flow rates in eq. (30) and iteratively solving the system of equations (29, 31-33) [13]:

$$K^i_{shift} = \frac{\left(\frac{n^i_{H_2}}{n^i_{tot} + 2\dot{r}^i_{ref}}\right) \cdot \left(\frac{n^i_{CO_2}}{n^i_{tot} + 2\dot{r}^i_{ref}}\right)}{\left(\frac{n^i_{CO}}{n^i_{tot} + 2\dot{r}^i_{ref}}\right) \cdot \left(\frac{n^i_{H_2O}}{n^i_{tot} + 2\dot{r}^i_{ref}}\right)} \quad (33)$$

Upon convergence in one slice, the resulting solution is used as initial guess to solve the same set of equations for the next computational slice. Similarly, the molar flow rates for the species flowing in the air channel are computed as

$$\begin{cases} \dot{n}^i_{N_2} = \dot{n}^{i-1}_{N_2} \\ \dot{n}^i_{O_2} = \dot{n}^{i-1}_{O_2} - 0.5 \cdot \dot{r}^i_{ox} \end{cases} \quad (34)$$

Energy Balance

The energy balance is applied by dividing the computational slice into three separate control volumes accounting for the solid trilayer and fuel and air channels (see **Figure 2**). Simplifying assumptions include the following: radiative effects between the solid trilayer and metallic interconnects are assumed negligible, although previous works [1, 4] suggest how considering the radiative heat transfer mechanism could enhance the model accuracy. This assumption will be indirectly validated in the Model Validation section by comparing with the work of Braun [1] that does take radiation into account (see Tables 9 and 10). Similarly, conduction in the solid trilayer in the flow direction is also neglected [4]. Hence, the dominant effects described in the model are the convective heat transfer between the solid trilayer and the fuel and air streams and the energy transfer due to the reactants and products fluxes.

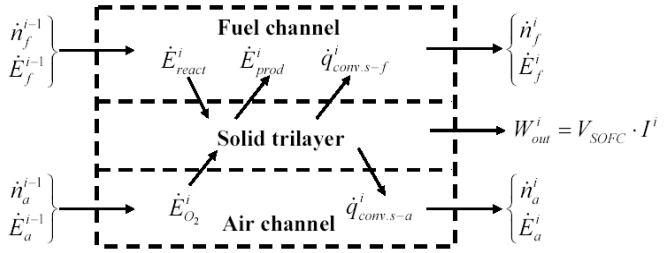

Figure 2 - Energy balance control volumes.

Applying the energy balance to the solid trilayer control volume (see Figure 3), the following balance is obtained:

$$\dot{E}^i_{in,\,ox}+\dot{E}^i_{in,\,ref}+\dot{E}^i_{in,\,shift}-\dot{q}^i_{conv,\,s-f}-\dot{q}^i_{conv,\,s-a}-\dot{E}^i_{el}=0 \qquad (35)$$

where, $\dot{E}_{in,ox}$, $\dot{E}_{in,ref}$ and $\dot{E}_{in,shift}$ represent the energy rates associated with oxidation, reforming, and shift reaction and are expressed by equations (36-38), respectively. $\dot{E}_{el}$ represents the power produced electrochemically in the solid trilayer and is expressed by equation (39):

$$\dot{E}^i_{in,ox}=\left[h_{H_2}(T^i_f)+\frac{1}{2}h_{O_2}(T^i_f)-h_{H_2O}(T^i_s)\right]\cdot\dot{r}^i_{ox} \qquad (36)$$

$$\dot{E}^i_{in,ref}=\left[h_{CH_4}(T^i_f)+h_{H_2O}(T^i_f)-3\cdot h_{H_2}(T^i_s)-h_{CO}(T^i_s)\right]\cdot\dot{r}^i_{ch_4} \qquad (37)$$

$$\dot{E}^i_{in,shift}=\left[h_{CO}(T^i_f)+h_{H_2O}(T^i_f)-h_{H_2}(T^i_s)-h_{CO_2}(T^i_s)\right]\cdot\dot{r}^i_{shift} \qquad (38)$$

$$\dot{E}^i_{el}=V_{SOFC}\cdot J^i\cdot A_{slice} \qquad (39)$$

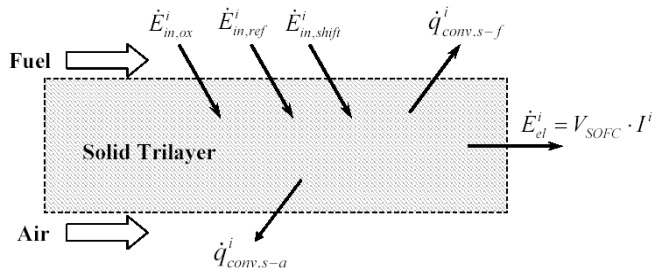

Figure 3 - Energy balance for the solid trilayer.

Convective heat transfer between the solid cell and the fuel/air channel is computed as:

$$q_{conv,s-f}=\bar{h}_f\cdot A_s\cdot(T^i_s-T^i_f) \qquad (40)$$

$$q_{conv,s-a}=\bar{h}_a\cdot A_s\cdot(T^i_s-T^i_a) \qquad (41)$$

The convective heat transfer coefficients, $\bar{h}_f$ and $\bar{h}_a$, are expressed as:

$$\bar{h}_f=\frac{N_u\cdot k_{gas}}{D_h} \qquad (42)$$

$$\bar{h}_a=\frac{N_u\cdot k_a}{D_h} \qquad (43)$$

where the hydraulic diameter D_h is given by [14]:

$$D_h=\frac{4\,A_{ch}}{2(l_{ch}+w_{ch})} \qquad (44)$$

and the Nusselt number N_u is evaluated as [1]:

$$Nu=7.541\cdot1-\left(2.61\cdot\beta+4.97\cdot\beta^2-5.119\cdot\beta^3+2.702\cdot\beta^4+0.548\cdot\beta^5\right) \qquad (45)$$

where β is the ratio between the channel height and the channel width. Following [1], the gas mixture thermal conductivity, k_{gas}, is calculated as a function of the thermal conductivity of each fuel gas specie:

$$k_{gas}=\sum_{i=1}^{n}\frac{y_i k_i}{\sum_{j=1}^{n}k_j A_{ij}} \qquad (46)$$

where

$$A_{ij}=\frac{\left[1+(k_i/k_j)^{1/2}.(M_j/M_i)^{1/4}\right]^2}{\left[8(1+M_i/M_j)\right]^{1/2}} \qquad (47)$$

and k_i (k_j) is the thermal conductivity of the *i-th* (*j-th*) specie.

Similarly, the energy balance equations developed for the control volumes around the fuel and air channels are represented, respectively, as

$$\dot{E}^{i-1}_f-\dot{E}^i_f+\dot{E}^i_{react}-\dot{E}^i_{prod}+\dot{q}^i_{conv\,,\,s-f}=0 \qquad (48)$$

$$\dot{E}^{i-1}_a-\dot{E}^i_a-\dot{E}^i_{O_2}+\dot{q}^i_{conv\,,\,s-a}=0 \qquad (49)$$

The energy balance equations, (35), (48) and (49), are solved simultaneously at each computational slice and the computed results are passed to the next slice in the flow direction once the isopotential criterion is satisfied, which serves as a check for the convergence of the procedure.

MODEL VALIDATION

The validation of the sub-models described above is accomplished by simulating SOFCs for 2 different sets of operating conditions. The first, developed at the PNNL [2], is a hydrogen-fueled SOFC unit that has been tested for different operating conditions in terms of nominal temperatures and average current densities, as reported in Table 6. This unit was operated at constant inlet fuel and air flows. An external cooling system was used in order to keep the operating temperatures constant. Accordingly, the solution of the energy balance described above is not required at a slice level. Using the PNNL data, it was possible to assess the polarization losses sub-model, as discussed below. The accuracy of the electrochemical model has been further investigated by carrying out a parametric analysis to estimate the influence of the main operating variables on the SOFC performance.

A second "virtual" SOFC unit has been simulated. Its specifications and operating conditions, reported in Table 8, were defined in 1995 by IEA. The simulation results have been compared with published data [1]. These data refer to a single operating current density (see Table 8), but assume that the IEA unit can be operated as an air-cooled system, and, moreover, as a pure hydrogen- or reformate-fueled fuel cell. Thus, not only was the validity of the energy balance sub-model developed

here demonstrated, but also it was possible to extend the 1-D model to the simulation of a reformate-fueled SOFC.

Numerical Solution

As noted in the modeling approach section, the spatial variation of the main operating variables of a SOFC is evaluated by discretizing the system in a number of computational slices and iteratively solving, for each slice, the governing equations (9), (35), (48) and (49). The inputs to the numerical procedure include the average current density drawn from the cell, fuel utilization and composition, excess air and air composition, inlet temperature for both air and fuel channels and the operating pressure. On output, the model provides the spatial distribution of the current density, temperature and species concentrations spatial distribution, operating voltage and electric power delivered by the cell.

The iterative procedure implemented in this work is based on the isopotential surfaces assumption: an initial guess of the first slice current density is used to calculate a voltage value, (considered invariant in the flow direction) in order to derive the current and temperature distributions. After all the slice balances are solved, the fuel utilization is evaluated and the procedure is repeated until the calculated U_f convergences to the input U_f.

Simulation of the PNNL unit

The system tested by PNNL is an anode-supported single SOFC. It is operated by feeding a very high constant amount of air and hydrogen, which results in limited oxygen depletion in the flow direction and very small fuel utilization, varying between 1% and 14% for a current density range (0.1-1) A/cm^2. As a consequence, the partial pressures of hydrogen and oxygen vary only slightly in the flow direction, so that the Nernst potential and the polarization losses are mostly affected by the operating temperature.

Table 6: PNNL SOFC specifications [2].

Geometrical data		
Electroactive area	3.8 cm^2	
Anode thickness	600 μm	
Cathode thickness	50 μm	
Electrolyte thickness	10 μm	
Anode porosity	0.30	
Cathode porosity	0.30	
Anode tortuosity	2.5	
Cathode tortuosity	2.5	
Operating Conditions		
Pressure	1 bar	
Temperature	[650 700 750 800] °C	
Fuel molar flow rates	$n_{H_2} = 1.44 \cdot 10^{-4}$ $n_{H_2O} = 4.46 \cdot 10^{-6}$	[mol/s]
Air molar flow rates	$n_{O_2} = 4.69 \cdot 10^{-5}$ $n_{N_2} = 1.76 \cdot 10^{-4}$	[mol/s]

The simulation results, obtained by iteratively solving the balances described above for a discretized cell of 20 slices are shown in Figure 4.

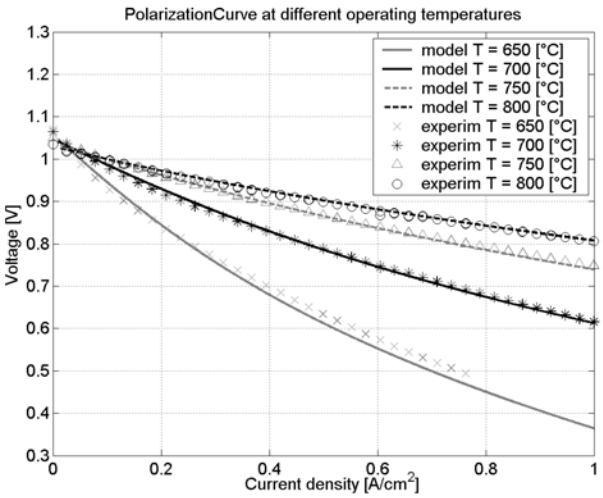

Figure 4 - Comparison between simulated and experimental data for the PNNL Solid Oxide test bench.

The comparison between the simulated and experimental data indicates that the model performs satisfactorily, with errors less than 3% over most of the investigated current range despite the fact that the coefficients in the polarization model (Tables 1 and 3) were only identified for an average current density of 0.5 A/cm^2. Furthermore, the shape of the V-I profiles agree with those reported in the literature [1, 10]. Figure 4 shows that the model is able to account for the temperature influence on the cell operating voltage. The operating temperature affects the cell voltage in two ways: the first effect is the reduction of the Nernst potential, because of the decrease of the Gibbs free energy and the increase of the second term on the right side of eq. (8); secondarily, a temperature increase enhances the diffusion and ionic conduction processes, thus resulting in a strong reduction of the activation, ohmic and concentration losses. As Figure 4 shows, the second positive effect fully compensates the small open circuit voltage reduction (i.e. Nernst potential).

Parametric analysis

In order to evaluate the effects of the main operating variables on SOFC performance, a parametric analysis was carried out on the PNNL unit. This analysis was conducted by varying fuel utilization, operating temperature and pressure around the nominal values of practical interest [1], as reported in Table 7. As for the PNNL validation step, the PNNL-electrochemical model and the mass-balance sub-models have been used to simulate the spatial-behavior of the SOFC unit. Due to the assumption of constant operating temperature in the flow direction, the energy balances do not need to be solved.

Table 7 : Operating-variable nominal values assumed for the parametric analysis.

Pressure	1 bar
Temperature	700 °C
Fuel utilization	0.75
Excess air	7
Inlet fuel composition	97% H_2, 3% H_2O

Figure 5 shows the influence of the operating temperature on the V-I profile. The temperature profiles are very similar to the ones depicted in Figure 4, thus confirming the overall

positive effect of an operating temperature increase on the SOFC performance. The cell voltage values reported in Figure 5 are lower than in Figure 4. This is due to the much higher fuel utilization value considered in the parametric analysis. The overall effect of U_f is explained below.

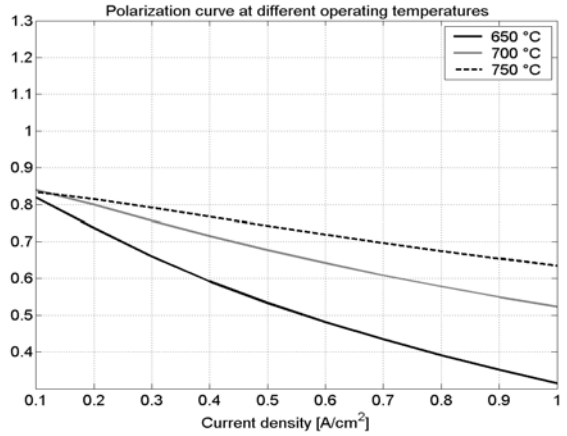

Figure 5 - Analysis of the operating temperature effect on the V-I profile for the PNNL SOFC.

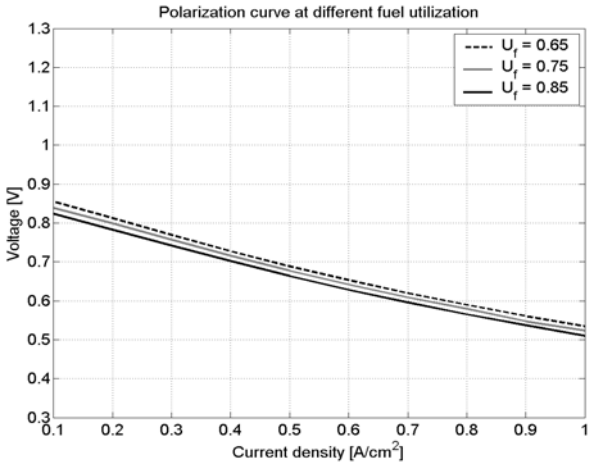

Figure 6 - Analysis of the fuel utilization effect on the V-I profile for the PNNL SOFC.

Figure 6 shows that a fuel utilization increase results in a cell voltage decrease throughout the whole current range. Figure 6 also shows that U_f has a linear influence on the V-I profile, since the three curves are almost equally spaced. The positive influence of decreasing U_f can be explained by considering the current distributions depicted in Figure 7. Since hydrogen decreases in the flow direction, less reactants are available, thus resulting in a monotonic decrease of the current density, as shown in Figure 7. Figure 7 also shows that a decrease in U_f results in a more uniform current distribution along the cell.

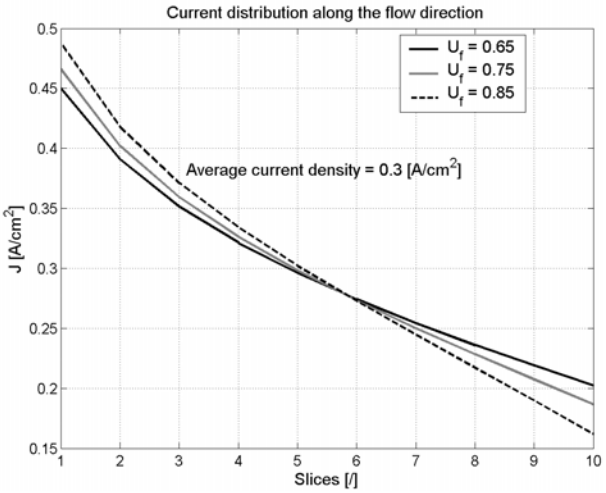

Figure 7 – Current evolution along the flow direction for different U_f values (PNNL system).

Since the electrode surfaces are isopotential, the effect of a U_f reduction on the cell voltage can be described by referring to the first computational slice, shown on Figure 7. At this location, the current density decreases as U_f decreases, corresponding to smaller polarization losses. On the other hand, at this location the Nernst potential does not change with U_f [3, 15], since the inlet partial pressures of the species at the anode depend only on the composition of the fuel fed to the cell. Thus, a lower fuel utilization results in a higher voltage for the overall cell.

Finally, Figure 8 describes the pressure effect on the SOFC performance. As expected, an increase in the inlet pressure produces an increase in the voltage for each operating current density. Pressure has a nonlinear effect on the V-I profiles. This behavior can be explained by referring to eq. (8), where the square root of the operating pressure appears at the denominator of the second term on the right side of the equation. Therefore, as pressure increases, the achievable voltage gain gradually decreases.

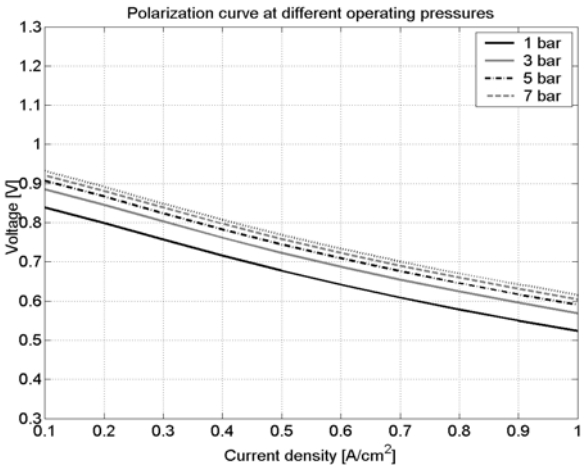

Figure 8 – Analysis of the operating pressure effect on the V-I profile for the PNNL SOFC.

Simulation of the IEA unit

The second application deals with the simulation of the virtual IEA unit, whose main assumptions are reported in Table 8 as described in [1].

Table 8: IEA SOFC specifications [1].

Geometrical data		
Electroactive area	100 cm^2	
Cell length	10 cm	
Anode thickness	50 μm	
Cathode thickness	50 μm	
Electrolyte thickness	150 μm	
Bipolar plates thickness	2500 μm	
Operating Conditions		
Pressure	1 bar	
Inlet Temperature	900 °C	
Fuel Utilization	85%	
Excess Air	7	
Average current density	0.3 A/cm^2	
Fuel feeding	**Pure-H_2**	**Reformate-fuel**
Inlet Fuel Composition	90% H_2 ; 10% H_2O	17.1% CH_4; 26.26% H_2; 49.34% H_2O; 2.94% CO; 4.36% CO_2.
Inlet Air Composition	21% O_2 ; 79% N_2	

The IEA unit is simulated for fueling from: A) pure hydrogen and B) reformate. Since the IEA unit is assumed to be air-cooled by feeding a large amount of excess air, the simulations of both case A and case B have been conducted by solving simultaneously the electrochemical, mass and energy balances for steady state conditions. The results obtained from the simulation of case A are summarized in Figure 9 and Table 9. In Figure 9 only the solid-trilayer temperature profile has been plotted, since the temperatures of the other control volumes (i.e. fuel and air channels) do not differ significantly, as already observed in previous studies [14].

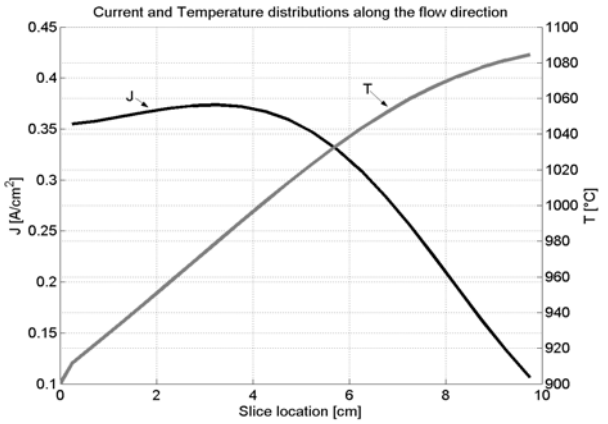

Figure 9 – Current and Temperature distributions simulated by the model for the pure H_2 fueled IEA SOFC.

As shown in Figure 9, the model predicts a temperature increase from the cell inlet to the outlet of about 170 °C, in agreement with the operational requirements in terms of cell component integrity at high temperatures. As can be seen from Figure 9, the temperature variation in the flow direction strongly influences the current density gradient. By comparison, for the constant-operating-temperature case simulated for the PNNL unit (see Figure 7), the model predicts a more uniform current distribution. The accuracy of the 1-D model has been verified by comparing the estimated output variables with the published data. Table 9 confirms that the model calculations fall within the ranges of values provided by the IEA test participants. Comparison between the present model and Braun results [1] shows that the simplified assumptions (*i.e.*, neglecting the radiative and conductive heat transfer mechanisms) are quite reasonable. The present results are in agreement with Burt et al. [4] indicating neglect of radiation results in a slightly higher outlet temperature.

Table 9 : Comparison between the IEA published data and the results obtained through the developed 1D Model for the hydrogen fueling case A.

	IEA ranges	**Model**	**Braun [1]**
Max J [A/cm^2]	[0.3725 - 0.3957]	0.3736	0.3799
Min J [A/cm^2]	[0.1020 - 0.1366]	0.1067	0.1211
Max T [°C]	[1048 - 1098]	1085	1059
Min T [°C]	[909 - 930]	911	924
Cell Voltage [V]	[0.702 – 0.722]	0.706	0.709
Output Power [W]	[21.06 - 21.67]	21.18	21.27

The reformate-fueling, case B, has been simulated using a U_f defined by eq. (4), in which the amount of the calculated methane has been assumed to be the input of a steam pre-reformer with a steam-carbon ratio of 2.5 to 1. This yields an inlet fuel flow rate with a composition that matches the IEA specifications reported in Table 8 [1].

Figure 10 and Figure 11 show the spatial distribution of temperature, current density and fuel gas molar fractions. Initially, the current density follows the temperature variation, which decreases significantly (about 50 °C) due to the highly endothermic methane reforming process. Then, after the methane is completely reformed, the temperature and hydrogen molar fraction increase, enhancing the electrochemical reactions. Thus, the current density increases reaching a maximum. Finally, due to the hydrogen consumption (see Figure 11), the current decreases monotonically to the cell outlet.

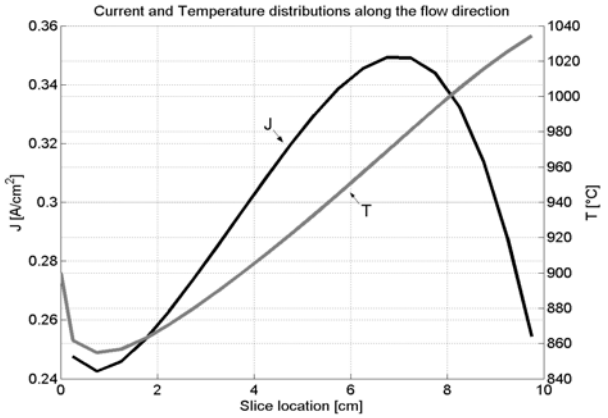

Figure 10 - Current and Temperature distributions simulated by the model for the reformate-fueled IEA SOFC.

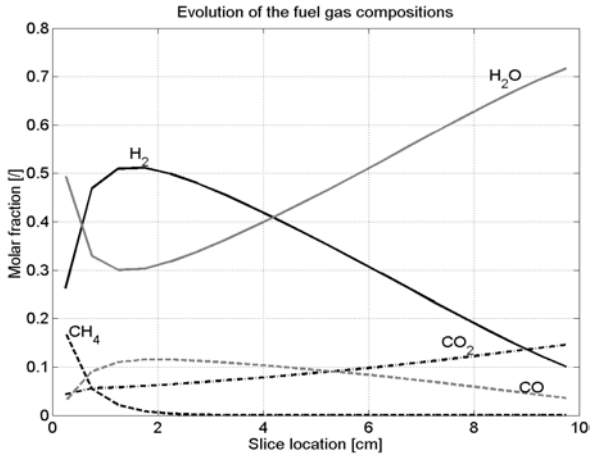

Figure 11 – Evolution of the fuel gas compositions estimated by the model for the reformate fueled benchmark.

As shown in Table 10, the comparison between the calculated and published SOFC output values confirms the good level of accuracy achieved and the validity of the model assumptions.

Table 10 : Comparison between the IEA published data and the results obtained through the developed 1D Model for the reformate fueling case B.

	IEA ranges	Model	Braun [1]
Max J [A/cm^2]	[0.3040 - 0.3665]	0.3492	0.3457
Min J [A/cm^2]	[0.1748 - 0.2508]	0.2425	0.2149
Max T [°C]	[1021 - 1034]	1034	1020
Min T [°C]	[847 – 862]	855	845
Cell Voltage [V]	[0.633 - 0.649]	0.644	0.650
Output Power [W]	[18.99 – 19.47]	19.24	19.49

CLOSURE

A 1-D model for simulating the main phenomena taking place in a single planar SOFC was presented in this paper. The 1-D model combines a phenomenological electrochemical model with appropriate forms of the conservation equations and aims to provide an accurate estimate of the spatial variation of the main SOFC operating variables for both hydrogen and reformate cases.

As described in the Introduction and Model Validation sections, validation of the model was successfully performed in two distinct phases based on previously published information. In work currently in progress, the overall model will be validated using data from an industrial partner that is not available for release at this time. This is expected to validate the model fully and provide a solid computational basis for incorporating the 1-D fuel cell model into system-level simulations, including balance of plant, involving automotive and military APU applications.

ACKNOWLEDGMENTS

This work was partially supported by a Grant from TACOM/NAC. The authors also would like to acknowledge the University of Salerno, Ohio State University Center for Automotive Research, the Saudi Government, Centro Ricerche Fiat (CRF) and Technical University of Denmark (DTU) for their support enabling the international collaborative work between the co-authors at Ohio State University.

REFERENCES

[1] Braun, R. J., 2002, "Optimal Design and Operation of Solid Oxide Fuel Cell Systems for Small-scale Stationary Applications,'' Ph.D. Thesis, University of Wisconsin, Madison, WI.

[2] Chick, L. A., Williford, R. E., Stevenson, J. W., Windisch Jr, C. F., and Simner, S. P., 2002, "Experimentally Calibrated, Spreadsheet Based SOFC Unit Cell Performance Model", *Fuel Cell Seminar Proceedings*, PNNL-SA-37014, 19-21 November, 2002, Palm Spring, CA.

[3] Haynes, C., 1999, "Simulation of Tubular Solid Oxide Fuel Cell Behavior for Integration Into Gas Turbine Cycles," Ph.D. Thesis, Georgia Institute of Technology, Atlanta, GA.

[4] Burt, A. C., Celik, I. B., Gemmenb, R. S., and Smirnov, A. V., 2004, "A numerical study of cell-to-cell variations in a SOFC stack," *Journal of Power Sources, Vol.126,* pp. 76–87.

[5] Chan, S. H., Khor, K. A., and Xia, Z. T., 2001, "A complete polarization model of a solid oxide fuel cell and its sensitivity to the change of cell component thickness," *Journal of Power Sources, Vol. 93***,** pp. 130-140.

[6] Achenbach, E., 1994, "Three-dimensional and time-dependent simulation of a planar solid oxide fuel cell stack", *Journal of Power Sources, Vol.49*, pp. 333–348.

[7] Singhal, S. C., and Kendall, K. (editors), 2003, "Solid Oxide Fuel Cells – Fundamentals, Design and Applications", Oxford, Elsevier Ltd., pp. 233-237.

[8] Chick, L. A., Williford, R. E., Stevenson, J. W., 2003, "Spreadsheet Model of SOFC Electrochemical Performance", SECA Modeling & Simulation Training Session August 2003 (web-page: www.netl.doe.gov/publications/proceedings/03/seca-model/seca-model03.html).

[9] Keegan, K., Khaleel, M., Chick, L. A., Recknagle, K., Simner S., and Deibler J., 2002, "Analysis of a Planar Solid Oxide Fuel Cell Based Automotive Auxiliary Power Unit", SAE Technical Paper Series No. 2002-01-0413, presented in SAE 2002 World Congress, March 4-7, 2002, Detroit, MI.

[10] Larminie, J., and Dicks, A., 2002, "Fuel Cell Systems Explained". John Wiley, Chichester, West Sussex.

[11] Cussler, E. L., 1984, "Diffusion – Mass transfer in fluid systems", Cambridge University Press, New York, NY, pp. 112-115.

[12] Achenbach, E., and Riensche, E., 1994, "Methane/steam reforming kinetics for solid oxide fuel cells," *Journal of Power Sources, Vol. 52***,** pp. 283-288.

[13] Massardo, A. F., and Lubelli, F., 2000, "Internal Reforming Solid Oxide Fuel Cell - Gas Turbine Combined Cycles (IRSOFC-GT). Part A: Cell Model and Cycle Thermodynamic Analysis", *ASME Transactions, Journal of Engineering for Gas Turbines and Power*, Vol. 122, pp. 27-35.

[14] Iwata, M., Hikosaka, T., Morita, M., Iwanari, T., Ito, K., Onda, K., Esaki, Y., Sakaki, Y., and Nagata, S., 2000, "Performance analysis of planar-type unit SOFC considering current and temperature distributions," *Solid State Ionics*, Vol. 132, pp. 297–308.

[15] Haynes, C. L., and Wepfer, W. J., 2000, "Enhancing Fuel Cell/ Gas Turbine Hybrid Power Systems via Reduced Fuel Utilization within Indirect Internally Reforming (IIR) Fuel Cell Stacks", *Proceedings of the ASME Advanced Energy Systems Division Publication AES*, CD-ROM, ASME, New York, Vol. 40, 2000.

